© 2016. Published by The Company of Biologists Ltd | Journal of Cell Science (2016) 129, 3309-3319 doi:10.1242/jcs.189258

RESEARCH ARTICLE

Divergence of structural strategies for homophilic E-cadherin binding among bilaterians

Shigetaka Nishiguchi[1,2,3], Akira Yagi[3], Nobuaki Sakai[3] and Hiroki Oda[1,2,*]

ABSTRACT

Homophilic binding of E-cadherins through their ectodomains is fundamental to epithelial cell–cell adhesion. Despite this, E-cadherin ectodomains have evolved differently in the vertebrate and insect lineages. Of the five rod-like, tandemly aligned extracellular cadherin domains of vertebrate E-cadherin, the tip extracellular cadherin domain plays a pivotal role in binding interactions. Comparatively, the six consecutive N-terminal extracellular cadherin domains of *Drosophila* E-cadherin, DE-cadherin (also known as Shotgun), can mediate adhesion; however, the underlying mechanism is unknown. Here, we report atomic force microscopy imaging of DE-cadherin extracellular cadherin domains. We identified a tightly folded globular structure formed by the four N-terminal-most extracellular cadherin domains stabilized by the subsequent two extracellular cadherin domains. Analysis of hybrid cadherins from different insects indicated that the E-cadherin globular portion is associated with determining homophilic binding specificity. The second to fourth extracellular cadherin domains were identified as the minimal portion capable of mediating exclusive homophilic binding specificity. Our findings suggest that the N-terminal-most four extracellular cadherin domains of insect E-cadherin are functionally comparable with the N-terminal-most single extracellular cadherin domain of vertebrate E-cadherin, but that their mechanisms might significantly differ. This work illuminates the divergence of structural strategies for E-cadherin homophilic binding among bilaterians.

KEY WORDS: Cadherin, Adherens junction, Cell adhesion, Atomic force microscopy, Insect, Evolution

INTRODUCTION

The main cell–cell adhesion molecules at adherens junctions are members of the classical cadherin family and are conserved across bilaterians (Harris and Tepass, 2010; Hulpiau and van Roy, 2009; Miller et al., 2013; Oda and Takeichi, 2011). The classical cadherins have a homophilic binding property that allows homogeneous cells to be organized into an independent solid tissue such as an epithelium (Nose et al., 1990; Takeichi, 1991; Vendome et al., 2014). Within the tissue, the extracellular bonds formed between the paired cadherins are thought to transmit forces originating from intracellular actomyosin activities that are required for epithelial homeostasis and morphogenesis (Borghi et al., 2012; Guillot and Lecuit, 2013; Heisenberg and Bellaïche, 2013; Takeichi, 2014).

[1]JT Biohistory Research Hall, 1-1 Murasaki-cho, Takatsuki, Osaka 569-1125, Japan. [2]Department of Biological Sciences, Graduate School of Science, Osaka University, Osaka, Japan. [3]R&D Group, Olympus Corporation, 2-3 Kuboyama-cho, Hachioji-shi, Tokyo 192-8512, Japan.

*Author for correspondence (hoda@brh.co.jp)

H.O., 0000-0003-4424-988X

Received 11 March 2016; Accepted 13 July 2016

Epithelial classical cadherins in vertebrates and insects, classified as type I and type IV cadherins, respectively, are commonly termed E-cadherins because they are functional counterparts at the adherens junctions in the major epithelial tissues of each organism; however, they have distinct domain organizations (Oda and Takeichi, 2011). The ectodomain of type I cadherin consists of five consecutive extracellular cadherin domains, referred to as EC1 to EC5. The ectodomain of type IV cadherin, as represented by the *Drosophila* E-cadherin, DE-cadherin (also known as Shotgun), instead has seven consecutive extracellular cadherin domains followed by a set of non-extracellular cadherin domains (Fig. 1A) (Oda and Tsukita, 1999; Oda et al., 1994, 2005). It has been suggested that the five and seven respective extracellular cadherin domains of type I and type IV cadherins have independently evolved from the common ancestral cadherin that is represented by type III cadherins (Hulpiau and Van Roy, 2010; Oda and Takeichi, 2011; Oda et al., 2005), which have 14–17 extracellular cadherin domains; a representative type III cadherin is *Drosophila* neural cadherin, DN-cadherin (also known as Cadherin-N) (Iwai et al., 1997; Tanabe et al., 2004). Notably, in some bilaterian animals such as echinoderms and spiders, type III cadherin appears to function as an 'E-cadherin' (Miller and McClay, 1997; Hiroki, 2012; Oda et al., 2005).

EC1–EC5 of type I cadherins exhibit a slightly curved, rod-like configuration in the presence of Ca^{2+} (Becker et al., 1989; Boggon et al., 2002; Pokutta et al., 1994). Individual extracellular cadherin domains adopt a seven-stranded β-barrel structure, and three Ca^{2+} ions are inserted into each inter-extracellular cadherin domain linker site, rigidifying the tandem structure (Nagar et al., 1996; Overduin et al., 1995; Shapiro et al., 1995). Of the five extracellular cadherin domains, the membrane-distal EC1 domain plays a pivotal role in the mechanism of homophilic binding, whereby β-strand-swapped dimers are formed between the EC1 domains of the paired cadherin molecules (Boggon et al., 2002; Häussinger et al., 2004; Shapiro et al., 1995). In this strand dimer interface, the side chain of a tryptophan residue at position 2 is inserted into a hydrophobic pocket of the partner EC1. Another type of adhesive dimer, termed the X-dimer, forms as a kinetic intermediate that precedes the formation of the strand-swapped dimer (Harrison et al., 2010). The binding interface of the X-dimer is localized around the Ca^{2+}-binding EC1–EC2 linker region and its binding affinity is relatively low. Vertebrate species contain multiple subtypes of type I cadherin (e.g. E-, P-, N- and R-cadherins), which mediate homophilic cell sorting behavior at least in cell culture conditions (Takeichi, 1990). The determinants responsible for their selectivity reside in their EC1 domains (Nose et al., 1990; Patel et al., 2006; Vendome et al., 2014), and small amino acid mutations in their EC1 domains can alter their binding specificities.

In contrast, our knowledge regarding the mechanism of homophilic cell–cell adhesion mediated by type IV cadherin is greatly limited. One notable finding has demonstrated that, upon

Journal of Cell Science (2016) 129, 3309-3319 doi:10.1242/jcs.189258

deletion of the other extracellular elements, the six consecutive N-terminal extracellular cadherin domains of DE-cadherin are capable of mediating homophilic adhesion both in cultured cells and in epithelial cells *in vivo* (Haruta et al., 2010). This capability is not seen when only four or five DE-cadherin N-terminal extracellular cadherin domains are used. Thus, the six N-terminal extracellular cadherin domains of DE-cadherin might constitute a functional unit involved in homophilic adhesion. The proposed evolutionary relationships between the extracellular cadherin domains of type III and type I cadherin, and between those of type III and type IV cadherin (Oda and Takeichi, 2011), indicate that the EC1 of type I cadherin and the EC6 of type IV cadherin evolved from the same extracellular cadherin domain in the common precursor. However, no tryptophan residue vital to strand swapping is found at the expected site in the EC6 or the N-terminal-most extracellular cadherin domain of type IV cadherins. Therefore, the mechanisms elucidated for type I cadherin binding are unlikely to be applicable to type IV cadherin.

In this study, to gain clues about the structural basis of homophilic adhesion mediated by type IV cadherin, we took two different approaches. First, we used atomic force microscopy (AFM) imaging to directly observe extracellular cadherin domains from DE-cadherin. We identified a tightly folded globular structure formed by the four N-terminal-most extracellular cadherin domains and stabilized by the subsequent two extracellular cadherin domains. Second, we applied a domain-swapping strategy to the type IV cadherins of three different insect species to identify the extracellular cadherin domains responsible for the homophilic binding specificity. We found that major determinants of homophilic type IV cadherin-binding specificities reside in the globular portion. Notably, the type IV cadherin EC2–EC4 region was identified as the minimal region capable of mediating an exclusively homophilic cell–cell binding specificity. Our findings illuminated the different structural strategies for E-cadherin homophilic binding between vertebrates and hexapods.

RESULTS

AFM imaging of extracellular cadherin domains in DE-cadherin

We first defined the ranges of the individual extracellular cadherin domains of DE-cadherin based on the conserved xPxF motif and designated them EC1 to EC7; for simplicity, we included the less characterized short N-terminal sequence (amino acids 70–87) of mature DE-cadherin in the EC1 domain (Fig. S1). We then expressed a DE-cadherin EC1–EC6 peptide (amino acids 70–733) tagged with 6×His at its C-terminus, referred to as DEEC6–His, in *Drosophila* S2 cells; this was followed by affinity purification (Fig. 1A; Fig. S2) and observation of its morphology by AFM in Ca^{2+}-containing buffer solution (Fig. 1B; Fig. S2). The majority of DEEC6–His proteins (>75%, n=34) exhibited a tadpole-like configuration, each consisting of a 'head' (or globular) and a 'tail' portion, although a small population of DEEC6–His proteins (~15%, n=34) exhibited a less obvious head–tail asymmetry. They all appeared as monomers. To locate the C-terminal EC6, we expressed and similarly examined a DE-cadherin EC1–EC6 peptide (amino acids 70–733) tagged with green fluorescent protein (GFP) and 6×His at its C-terminus (Fig. 1A; Fig. S2), referred to as DEEC6–GFP–His. DEEC6–GFP–His formed virtually the same configuration as DEEC6–His, except that it demonstrated an additional spherical object at the tail end (Fig. 1C; Fig. S2), which likely corresponded to the GFP portion. However, although the length of the long axis of GFP is known to be 4 nm or slightly less (Yang et al., 1996), the presumable GFP portions of DEEC6–GFP–His molecules were viewed as larger than 4 nm (up to ~15 nm) in length. This discrepancy might be attributed to the scanning tip geometry (i.e. tip shape and sharpness), which affects the resolution and length measurement in AFM imaging (Vesenka et al., 1993). In principle, when a rigid object is scanned with a more blunt tip, it is viewed as larger at a lower resolution. Although the radius of curvature of the scanning tips we used was likely to be less than 10 nm, the sharpness of the individual scanning tips, which need to be replaced in each experiment, appeared to vary within the range. In addition, scans with a sharper tip might have more chances to damage the specimen (Vesenka et al., 1993). The resolution and quality of the AFM images of DEEC6–His and DEEC6–GFP–His, therefore, unavoidably varied from one experiment to another (Fig. S2). However, whereas these considerations indicate the technical limitations of AFM imaging with respect to the accurate determination of the size of a molecule, the reproducible difference observed between the shapes of DEEC6–His and DEEC6–GFP–His led us to conclude that EC6 is located at the end of the tail portion of DEEC6–His.

DEEC6–His and DEEC6–GFP–His had convex and nonconvex sides (Fig. 1B,C), allowing us to define the head–tail and convex–nonconvex axes. In almost all molecules displaying tadpole-like shapes, the same lateral side with respect to the HT and CN axes faced the front (opposite to the mica surface) (Fig. S2). We defined this side as the left side. The nonrandom orientation of the molecules might have resulted from uneven affinities of the left and right sides of the molecules for the mica surface and/or biased behaviors of the molecules in the gravitational field.

Despite the limited accuracy described above, we carried out length measurements using twenty selected AFM images of tadpole-shaped DEEC6–His molecules obtained with a scanning tip considered likely to be sharp. The mean length of DEEC6–His along the circumference of a circle fitting its curved configuration measured ~26 nm (n=20), a value that is equal to ~5.8 times the typical extracellular cadherin domain length (4.5 nm) (Shapiro et al., 1995). However, given that the measured length value in AFM imaging depends on the scanning tip geometry as previously noted, the actual length value is likely to be less than 26 nm. The head and tail portions occupied, on average, 56% and 44%, respectively, of the entire length. The width of DEEC6–His in the middle of the head portion was, on average, 1.3 times as large as that in the middle of the tail portion. These measurements suggest that the six consecutive extracellular cadherin domains of DEEC6–His are folded rather than extended. Furthermore, AFM imaging of DEEC6–His at a higher resolution allowed us to recognize two morphological segments in the tail portion (Fig. 1D,E) that most likely correspond to EC5 and EC6. We considered, therefore, that the globular portion of DEEC6–His consists of the N-terminal four extracellular cadherin domains. Notably, we had rare chances to observe the globular portion of DEEC6–His turning over, while acquiring serial images (Fig. 1F,G). The morphology of DEEC6–His viewed from its right side revealed a J-shaped strand of consecutive extracellular cadherin domains, in which the likely N-terminal region was distinctly segmented and tightly associated with the convex-side extracellular cadherin domains.

To confirm the foldability of the DE-cadherin EC1–EC4 region, we expressed DE-cadherin EC1–EC4 peptides (amino acids 70–522) tagged with 6×His, or with GFP and 6×His, at their C-termini (Fig. 1A; Fig. S2), referred to as DEEC4–His and DEEC4–GFP–His, respectively, and examined them by AFM. DEEC4–His molecules showed varied morphologies; some were

Journal of Cell Science (2016) 129, 3309-3319 doi:10.1242/jcs.189258

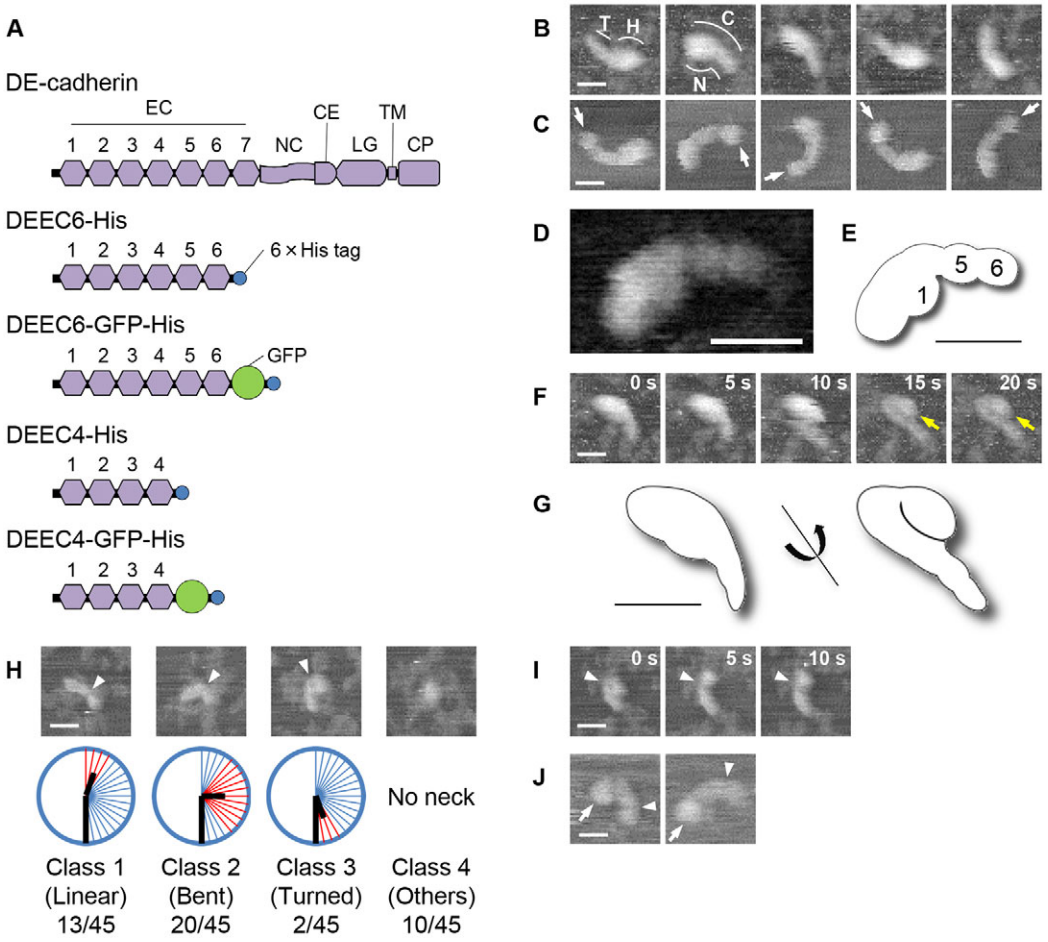

Fig. 1. AFM imaging of the extracellular cadherin domains of DE-cadherin. (A) Schematic representation of mature DE-cadherin, DEEC6–His, DEEC6–GFP–His, DEEC4–His and DEEC4–GFP–His. EC, extracellular cadherin domain; NC, nonchordate-specific classical cadherin domain; CE, cysteine-rich EGF-like domain; LG, laminin globular domain; TM, transmembrane domain; and CP, cytoplasmic domain. The N-terminal region (amino acids 1–69) that is removed during maturation (Oda and Tsukita, 1999) is not depicted. (B,C) Representative images of DEEC6–His (B) and DEEC6–GFP–His (C) molecules. The head (H) and tail (T) portions and the convex (C) and nonconvex (N) sides of DEEC6–His are indicated. In the rightmost DEEC6–His molecule, the H–T asymmetry is less obvious. Arrows in C point to the presumed GFP portion of each DEEC6–GFP–His molecule. See Fig. S2 for more examples. (D,E) High-resolution image (D) and interpretive illustration (E) of a DEEC6–His molecule. The numbers indicate the positions of the numbered extracellular cadherin domains. (F,G) Timecourse (F) and schematic illustrations (G) of a DEEC6–His molecule whose head portion was turning over. Yellow arrows in F point to the N-terminal segment clearly visible on the nonconvex side of the molecule. (H) Images showing distinct morphologies of different DEEC4–His molecules. Arrowheads point to the 'neck' of each molecule. The molecules were classified into four classes based on the presence or absence of a recognizable neck and the degree of bending at the neck (red lines): class 1, linear; class 2, bent; class 3, turned; and class 4, others (no neck recognized). The molecule count for each class is shown, which was obtained from three separate square regions representing a total of 45 molecules. See Fig. S2 for details. (I) Timecourse of a DEEC4–His molecule undergoing morphological changes. (J) Images of DEEC4–GFP–His molecules. Arrowheads in I and J point to the 'neck' of each molecule as in H. Arrows in J point to the presumed GFP portion of each DEEC4–GFP–His molecule. Scale bars: 10 nm.

bent and others were crescent-shaped or extended more linearly (Fig. 1H; Fig. S2). Irrespective of their overall shapes, many of these molecules (78%, n=45) exhibited a 'neck' at about one third of the length. The neck-bearing molecules were classified based on the degree of bending at the neck (Fig. 1H; Fig. S2). Approximately 60% of the neck-bearing molecules were distinctly bent or turned at the neck, whereas the remaining 40% were linear or slightly bent. In addition, a timecourse analysis of a DEEC4–His molecule showed that the neck acted as a flexible hinge (Fig. 1I). Comparison of the morphologies of DEEC4–His with those of DEEC4–GFP–His provided topological information (Fig. 1H,J), which indicated that the position of the neck is closer to the N-terminal end than to the C-terminal end of the EC1–EC4 region. These observations clearly show that the DE-cadherin EC1–EC4 domain is foldable, possibly with a hinge formed at or near the EC2. They also suggest that the formation and stabilization of the tightly packed globular arrangement of the DE-cadherin EC1–EC4 region requires the whole or a part of EC5–EC6.

Determination of the extracellular cadherin domains responsible for homophilic binding specificity by performing analysis of hybrid E-cadherins from different insect species

Next, we pursued the functional significance of the observed structural features of DE-cadherin by conducting a domain-swapping analysis between type IV cadherins of different insect species (Fig. 2A). The full-length constructs of DE-cadherin and *Gryllus bimaculatus* (cricket) type IV cadherin, Gb1-cadherin, referred to as DEFL and Gb1FL, respectively, exhibited mutually exclusive adhesion specificities (Fig. 2B–D). All the extracellular cadherin domains of DE- and Gb1-cadherins have amino acid sequences that can be unambiguously aligned, albeit with a considerable degree of divergence (49.7% identity) (Fig. S1). Of

Journal of Cell Science (2016) 129, 3309-3319 doi:10.1242/jcs.189258

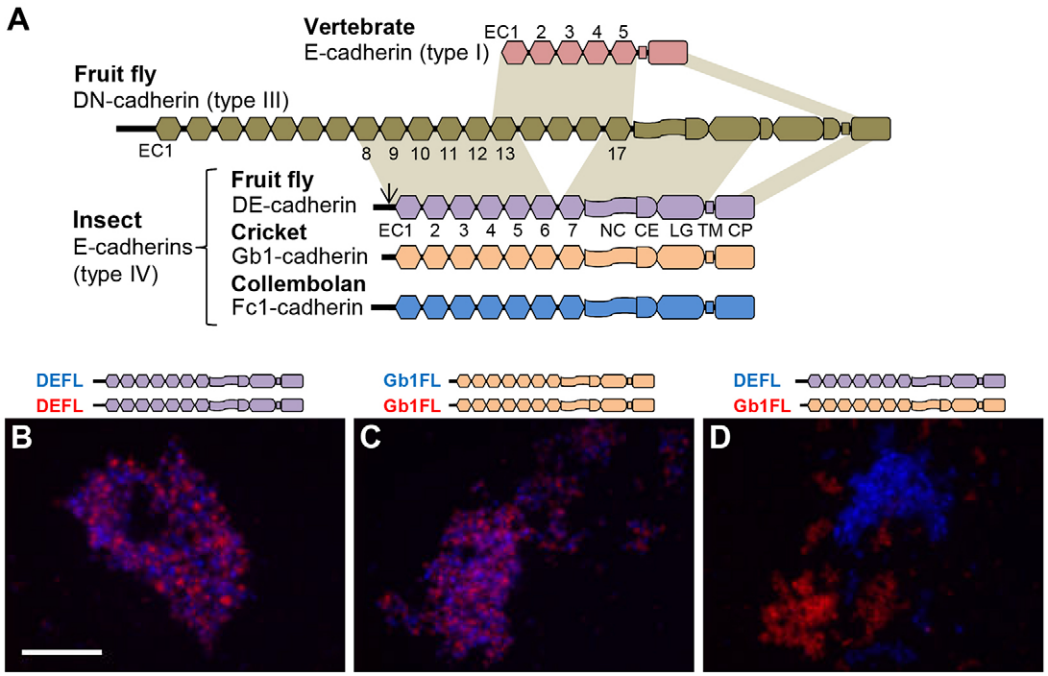

Fig. 2. DE-cadherin and Gb1-cadherin exhibit different homophilic binding specificities. (A) Schematic illustrations showing the relationships between the domain structures of vertebrate E-cadherin, DN-cadherin and insect E-cadherins (labeled as in Fig. 1A). The arrow denotes the proteolytic site for removal of the signal peptide. The likely homologous regions between type I, type III and type IV cadherins are indicated by shading (Oda and Takeichi, 2011). (B–D) Representative images of mixed cell aggregation assays using cells expressing DEFL (B,D) or Gb1FL (C) and TagBFP (blue) and those expressing DEFL (B) or Gb1FL (C,D) and mKate2 (red). Scale bar: 30 µm.

the seven extracellular cadherin domains, EC2 showed the least conservation between DE- and Gb1-cadherins (38.5% amino acid identity). To identify the key extracellular cadherin domains responsible for the different binding specificities of the different type IV cadherins, we constructed a series of DE-cadherin–Gb1-cadherin hybrid molecules (Fig. 3A; Fig. S3) using DEFL and Gb1FL as the parent constructs and DNFL, a DN-cadherin construct, serving as a negative control.

First, we examined the capability of each construct to mediate cell aggregation on its own. Based on the sizes of the largest cell aggregates formed in the cell aggregation assays using S2 cells, three categories for the levels of homophilic cell–cell binding capabilities were defined (Fig. 3B; Fig. S4). Seven of the fourteen DE-cadherin–Gb1-cadherin hybrids retained moderate or high levels of homophilic binding capabilities, whereas the others showed grossly reduced or no detectable homophilic binding capabilities. However, despite the complicated nature of the results, it was clear that the exchange of the N-terminal four extracellular cadherin domains between DE- and Gb1-cadherins did not significantly affect the homophilic binding capability.

Next, we quantified the binding preferences of each construct to DEFL (P_D), Gb1FL (P_G), or DNFL (P_N) (Fig. 3C; Fig. S4). Mixed aggregation assays were conducted using S2 cells expressing construct X and mKate2 and those expressing DEFL, Gb1FL or DNFL, and TagBFP at a 1:4 density ratio. The binding preferences were calculated from the intensities of mKate2 and TagBFP fluorescence in the formed cell aggregates (Fig. 3D; Fig. S4). For D4, the P_D and P_G values were 1.07±0.08 and 0.02±0.01 (mean± s.e.m., n=3), respectively, and those for G4 were 0.07±0.02 and 0.94±0.07 (n=3), respectively, indicating that the EC1–EC4 region of each type IV cadherin contains most, if not all, of the determinants specifying exclusive binding to the same cadherin.

The results from other constructs wherein three or fewer extracellular cadherin domains of the EC1–EC4 region were replaced, however, were highly complicated. This is possibly due to partial or total disruption of binding specificity determinants. Nonetheless, we could deduce information regarding the contributions of the individual extracellular cadherin domains by comparing the preference values between mutually similar, but not identical, constructs (Fig. 3C; Fig. 4). As revealed by G1, D1G2, D12G3 and D123G4, none of the DE-cadherin EC1, EC2, EC3 and EC4 regions were essential for associating with DEFL (Fig. 3C; Fig. 4). This indicates that we failed to narrow down the specificity-determination to any single extracellular cadherin domain. Nonetheless, the different EC1 domains between DEFL and G1 and between D4 and G1D234 produced opposite effects on P_D and P_G (Fig. 3C; Fig. 4), wherein DE-cadherin EC1 increased and decreased P_D and P_G, respectively, whereas Gb1-cadherin EC1 decreased and increased these values. This suggests the EC1 regions contribute to the binding specificities. Despite this, the presence of a single DE-cadherin EC1 in a Gb1-cadherin background (D1) was not capable of inducing any association with DEFL, implying that DE-cadherin EC1 might depend on other DE-cadherin extracellular cadherin domains for its contribution toward generating DE-cadherin specificity. However, the presence of a single Gb1-cadherin extracellular cadherin domain in a DE-cadherin background (G1) was capable of inducing association with Gb1FL to some extent, implying that Gb1-cadherin EC1 might possess an activity independent of other Gb1-cadherin extracellular cadherin domains with respect to its contribution to generating Gb1-cadherin specificity. Thus, these data were not symmetrical between the two type IV cadherins of different species, indicating the existence of a species-specific mechanism.

Journal of Cell Science (2016) 129, 3309-3319 doi:10.1242/jcs.189258

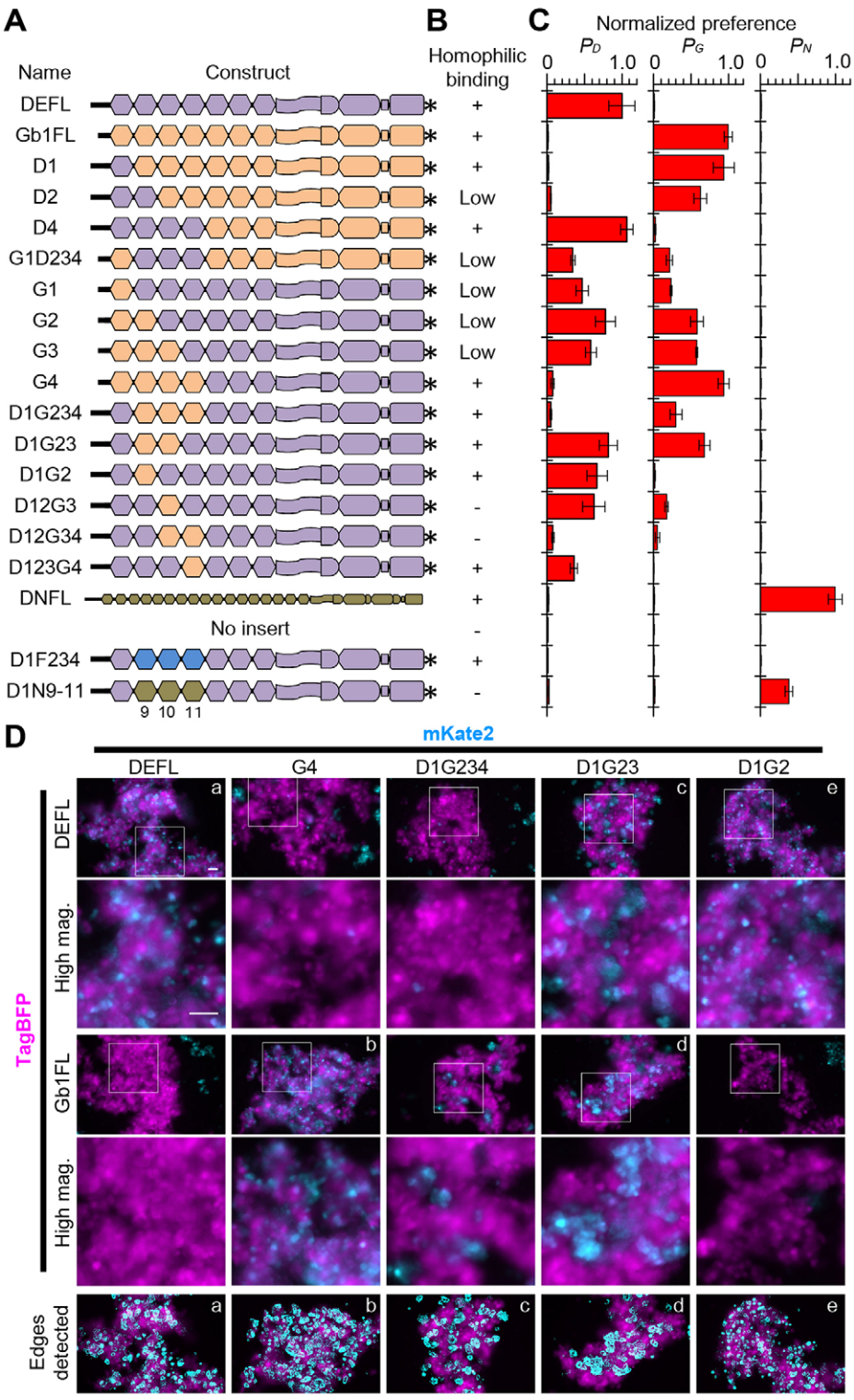

Fig. 3. Characterization of the binding properties of the constructed hybrid cadherins. (A) Schematic representation of parent and hybrid cadherin constructs. The domains are color-coded as in Fig. 2A to indicate their sources. Asterisks indicate tagged GFP. (B) Levels of homophilic binding capability. The levels were categorized into three classes: class 1, high or moderate (+); class 2, detectable but low (Low); and class 3, not detectable (–) (see Fig. S4 for details). (C) Quantification of the binding preferences to DEFL (P_D), Gb1FL (P_G) and DNFL (P_N). Three independent transfections were performed for each construct. The values are normalized to those of DEFL, Gb1FL or DNFL and are represented as the mean±s.e.m. (D) Representative images of cell aggregates formed in mixed aggregation assays. Cells expressing the indicated constructs (labeled with mKate2, cyan) and those expressing DEFL or Gb1FL (labeled with TagBFP, magenta) were mixed. The boxed regions are magnified in the lower panels. mKate2 fluorescence images in the panels indicated by a–e were subjected to edge detection and then recombined with the TagBFP fluorescence images. The resulting images are displayed at the bottom; these facilitate recognition of the distributions of single or clustered mKate2-positive cells in the co-aggregates. Scale bar: 50 µm.

Notably, the different EC3–EC4 domains between D2 and D4, G2 and G4, and even the different EC4 domains between G3 and G4 oppositely affected P_D and P_G (Fig. 3C; Fig. 4). In addition, EC4 comparisons between DEFL and D123G4, D1G234 and D1G23, and D12G3 and D12G34 showed that DE-cadherin EC4 facilitated stronger associations with DEFL. These results were consistent with the epitope position of the anti-DE-cadherin monoclonal antibody DCAD1, which is capable of inhibiting DE-cadherin-mediated cell aggregation (Oda et al., 1994; Fig. S3; see Materials and Methods). Furthermore, the ability of D1G23 and D12G3 to demonstrate preferences for Gb1FL appeared to depend on the Gb1-cadherin EC3 region (Fig. 3C; Fig. 4). Taken together, these results suggest that the EC3–EC4 domain do contribute to the cadherin-binding specificities.

Among the DE-cadherin–Gb1-cadherin hybrid with homophilic binding capabilities, D1G23 and D1G234 were found to exhibit peculiar binding properties. Although D1G23-expressing cells coaggregated with both DEFL-expressing and Gb1FL-expressing

Journal of Cell Science (2016) 129, 3309-3319 doi:10.1242/jcs.189258

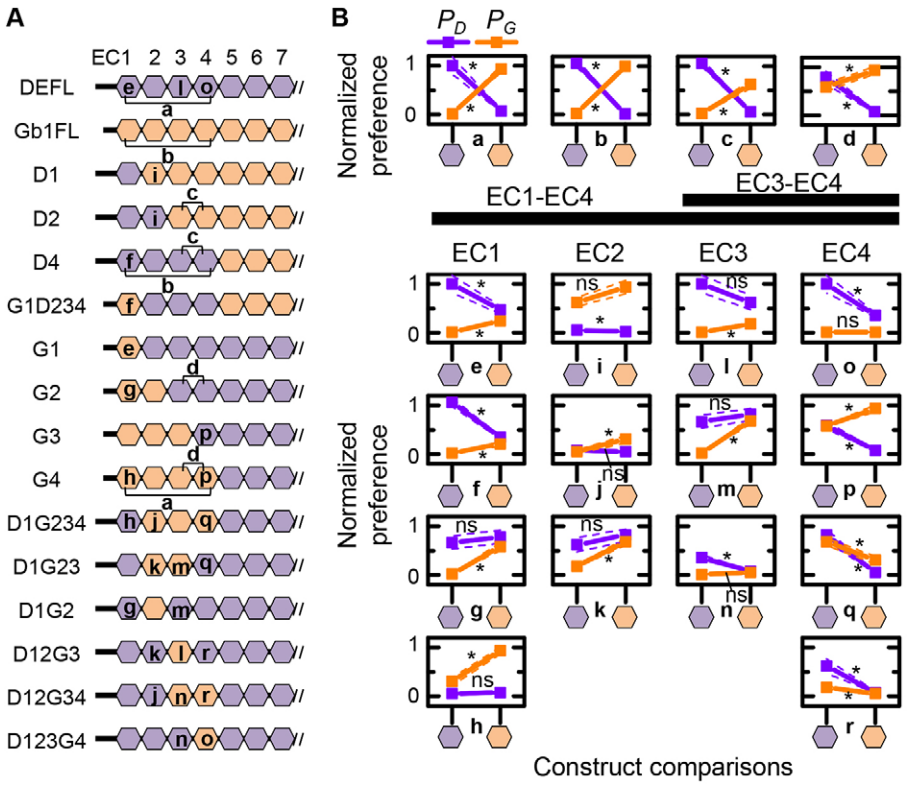

Fig. 4. Statistical evaluation of the binding preferences exhibited by related constructs of DE-cadherin and Gb1-cadherin. The data shown in Fig. 3C were analyzed. (A) Schematic representation of the compared cadherin constructs. The NC domain and the more C-terminal regions of each construct are not shown. The extracellular cadherin domains from DE-cadherin are displayed in purple and those from Gb1-cadherin in orange. The same lowercase letters indicate the different single or multiple extracellular cadherin domains of the two mutually similar constructs that were compared. (B) Tests of the significance of the differences between the binding preferences of mutually similar cadherin constructs. Each graph represents the normalized preferences, P_D (purple) and P_G (orange), of two cadherin constructs indicated by the same lowercase letter in A. Dotted lines indicate the s.e.m. The slopes of the colored lines indicate the differences between the P_D or P_G values of the paired constructs. *P<0.05; ns, not significant (Welch's t-test).

cells, they did not intermingle randomly but contained many small homoaggregates of D1G23-expressing cells (Fig. 3D). This situation sharply contrasted with cells expressing DEFL, G4 and D1G2, and indicated that D1G23 prefers homophilic associations to heterophilic associations with DEFL and Gb1FL. In comparison, the behaviors of D1G234-expressing cells appeared to be more extreme in terms of self-preference. Despite being able to form self-aggregates, they could not generate co-aggregates with DEFL-expressing cells and only a few were incorporated into the aggregates of Gb1FL-expressing cells. These notable behaviors of D1G234-expressing cells, which might imply the creation of a new homophilic specificity, were captured in the P_D and P_G values as compared between D1G23 and D1G234 (Fig. 4). These findings prompted us to test whether the EC2–EC4 region of type IV cadherin constitutes a replaceable unit capable of mediating homoassociations in a DE-cadherin background.

To this end, we constructed a DE-cadherin wherein EC2–EC4 was replaced with the homologous region of the *Folsomia candida* (collembolan) type IV cadherin Fc1-cadherin (referred to as D1F234; Fig. 2A; Fig. 3A). This hybrid cadherin exhibited a homophilic binding capability with no preference for DEFL, Gb1FL or DNFL (Fig. 3B,C; Fig. S4). DEFL, D1G234, and D1F234 are identical except in their EC2–EC4 regions. We then conducted mixed aggregation assays using cells expressing these cadherins, which showed that distinct aggregates were formed depending on the cadherin constructs utilized (Fig. 5A–C). This indicated that the cells expressing each construct exhibited a substantial level of self-preference, suggesting that the EC2–EC4 region of insect E-cadherin represents the minimal portion capable of mediating an exclusive homophilic binding specificity.

In addition, G1D234, an inverted construct of D1G234, retained a preference for Gb1FL as did G1, possibly owing to the presence of Gb1-cadherin EC1, but failed to exhibit a substantial level of homophilic binding capability (Fig. 3B,C; Fig. S4). It was therefore not possible to test the capability of a type IV cadherin EC2–EC4 region in a Gb1-cadherin background.

Conservation of the specificity-determining extracellular cadherin domains between type IV and type III cadherins

In a previous study (Oda et al., 2005), the amino acid sequences of the individual extracellular cadherin domains of type IV and type III cadherins were systematically compared to elucidate the structural and evolutionary relationships between the two cadherin types, which suggested that the EC2–EC4 region of type IV cadherin is homologous to the EC9–EC11 region of type III DN-cadherin (Fig. 2A; Fig. S1). To test the possibility that the EC9–EC11 region of DN-cadherin might have a similar function to that of the EC2–EC4 region of type IV cadherin, we constructed another DE-cadherin wherein EC2–EC4 was replaced with the homologous region of DN-cadherin (referred to as D1N9-11; Fig. 2A; Fig. 3A). Although this hybrid cadherin had no homophilic binding capability, it was capable of mediating associations with DNFL but not with DEFL or Gb1FL (Fig. 3B,C; Fig. 5D–F; Fig. S4). These results demonstrate that type IV and type III cadherins have three consecutive evolutionarily conserved extracellular cadherin domains through which they can specifically recognize and bind the same cadherins.

DISCUSSION

Our AFM imaging of the extracellular cadherin domains of DE-cadherin provides the first example of a tightly and stably folded globular structure organized by multiple consecutive extracellular cadherin domains. Notably, our analyses of hybrid cadherins associated the identified globular portion of the insect E-cadherin with the determinants of homophilic binding specificity. These findings shed light on the differences in the structural bases for

Journal of Cell Science (2016) 129, 3309-3319 doi:10.1242/jcs.189258

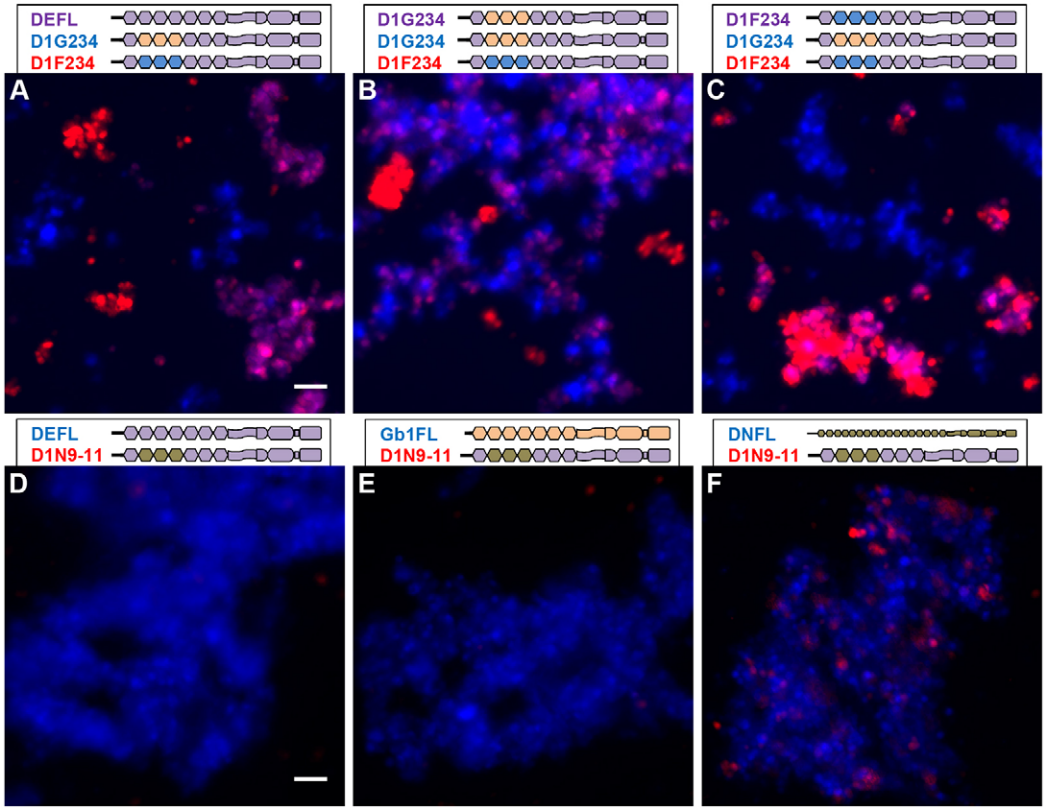

Fig. 5. Identification of the different binding specificities mediated by the three consecutive mutually homologous extracellular cadherin domains of different type IV and type III cadherins. (A–C) Mixed cell aggregation assays using cells expressing DEFL, D1G234 or D1F234. The three cell populations were identified by co-expression of a mixture of TagBFP and mKate2 (purple), TagBFP only (blue), or mKate2 only (red) (A), as indicated. In the controls, D1G234 (B) or D1F234 (C) was used instead of DEFL. (D–F) Mixed cell aggregation assays using cells expressing D1N9-11 and those expressing DEFL (D), Gb1FL (E) or DNFL (F). Two cell populations were identified by coexpression of mKate2 only (red) and TagBFP only (blue) as indicated. Scale bars: 50 µm.

homophilic cell–cell adhesion mediated by insect and vertebrate E-cadherins (Fig. 6A,B). Furthermore, as shown in previous structural studies on vertebrate E-cadherins, the linkers between typical extracellular cadherin domains allow structural rigidification by Ca^{2+} insertions, which accounts for the extended, rod-like configuration of the five tandem extracellular cadherin domains of the vertebrate E-cadherins (Nagar et al., 1996; Pokutta et al., 1994). The EC2 and EC3 of DE-cadherin and the corresponding consecutive extracellular cadherin domains of its insect orthologs are, however, atypical extracellular cadherin domains in that their linker regions lack Ca^{2+}-binding motifs or residues (Jin et al., 2012; Fig. S1). Crystallographic and electron microscopic studies on consecutive extracellular cadherin domains with similar, but not homologous, Ca^{2+}-free inter-extracellular cadherin domain linkers in DN-cadherin and non-classical cadherins has suggested that such Ca^{2+}-free inter-extracellular cadherin domain linkers are involved in the bending of the extracellular cadherin domain strands (Jin et al., 2012; Tsukasaki et al., 2014), although the relevance of the bent structures to adhesion was not demonstrated. Taking these previous studies into account, it is highly possible that the divergent EC2–EC3 linker of DE-cadherin is involved in the observed foldability of its EC1–EC4 region (Fig. 6A).

Our systematic domain-swapping analyses revealed that the N-terminal-most four extracellular cadherin domains of type IV cadherin include major determinants of its homophilic binding specificity. However, this region is not sufficient to mediate cell–cell adhesion as both EC5 and EC6 are required to achieve adhesion (Haruta et al., 2010). These findings might be associated with our observations that revealed a possible contribution of EC5–EC6 to stabilizing the folded state of the EC1–EC4 region.

From a functional viewpoint, the N-terminal four extracellular cadherin domains of the insect E-cadherin are comparable with the N-terminal EC1 of vertebrate E-cadherin (Fig. 6A,B), given that both regions form the core determinants of their respective homophilic binding specificities. Notably, our finding of mutually exclusive binding specificities of DEFL, D1G234 and D1F234 suggested that the EC2–EC4 region of a type IV cadherin is capable of specifically and exclusively recognizing the same region of the same cadherin, as its binding partner. Adhesive bonds might form between these regions of paired type IV cadherin molecules. We initially expected to observe dimers of purified DE-cadherin extracellular cadherin domains in solution by AFM; however, only monomers were detected. AFM observation of dimers of purified VE-cadherin (type II cadherin) ectodomains has been previously reported (Brasch et al., 2011), suggesting that the individual binding interactions of the DE-cadherin peptides might be relatively weak. Alternatively, the conditions during sample purification and preparation might prevent the DE-cadherin peptides from being fully functional. Nevertheless, an independent line of evidence exists that supports the importance of the EC4 in the homophilic binding interactions of DE-cadherin ectodomains. The epitope of the anti-DE-cadherin monoclonal antibody DCAD1, which is capable of inhibiting DE-cadherin-mediated cell re-aggregation (Oda et al., 1994), was found to be located in the EC4–EC5 junction region (Fig. S3). Furthermore, the data obtained with the hybrid construct D1G23 have implications

Journal of Cell Science (2016) 129, 3309-3319 doi:10.1242/jcs.189258

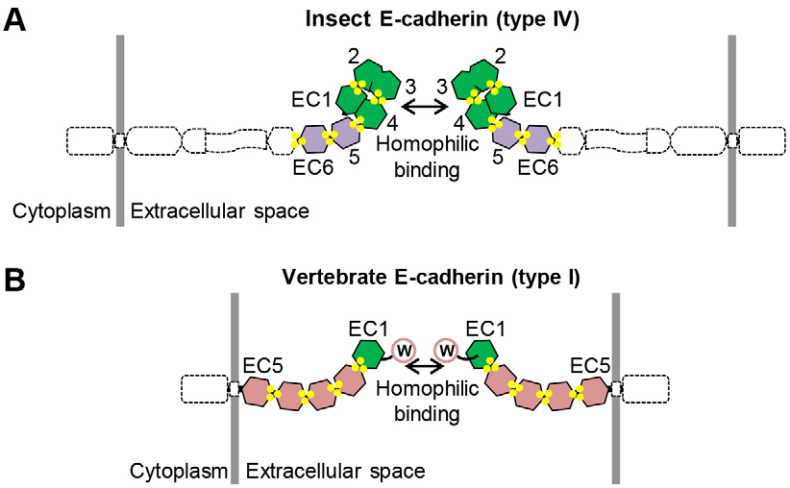

Fig. 6. Different structural strategies for homophilic binding of insect and vertebrate E-cadherins through their ectodomains. (A) A proposed model of a folded arrangement of the six consecutive N-terminal extracellular cadherin domains of insect E-cadherin. (B) The general model of a slightly curved, tandem arrangement of the five consecutive extracellular cadherin domains of vertebrate E-cadherin. Only the molecular domains focused on in this work are displayed in color. The extracellular cadherin domains shown in green serve analogously as the determinants of homophilic binding specificities. Yellow dots indicate Ca^{2+} ions that are inserted into the linker regions of the neighboring extracellular cadherin domains to rigidify the tandem structures of the consecutive extracellular cadherin domains. As an exception, the Ca^{2+}-free EC2–EC3 linker of insect E-cadherin might confer foldability on the consecutive extracellular cadherin domains. The EC2–EC4 region of insect E-cadherins plays a primary role in mediating the homophilic binding specificity, with EC1 playing a supportive role. In addition, the EC1 domain of vertebrate E-cadherin contains a conserved tryptophan residue (W) inserted into the hydrophobic pocket (not depicted) in the EC1 of the partner cadherin.

for the topology of the homophilic binding interactions. The reasonable assumption that the observed preferential homo-associations of D1G23-expressing cells result from the optimal interactions between the same-species portions of the hybrid molecules predicts that the EC2–EC4 regions of the paired type IV cadherins might associate with each other in a parallel, rather than in an antiparallel, orientation (Fig. 6A). If this is the case, then the folded conformation of the EC1–EC4 region might facilitate the participation of the EC1 domain in the mechanism of homophilic binding. Consistent with this, our data from the D1, D2, and D4 constructs showed that DE-cadherin EC1 depends on DE-cadherin EC3–EC4 for its contribution to generating DE-cadherin binding specificity. We thus suggest that the EC2–EC4 region plays a primary role in the homophilic binding of type IV cadherin, whereas the EC1 domain modifies and/or ensures the binding specificity. These predictions need to be tested in future experiments using more detailed structural studies.

The DE-cadherin EC2–EC4 region is evidently homologous to the DN-cadherin EC9–EC11 region, although the two *Drosophila* classical cadherins have different total numbers of extracellular cadherin domains (Oda et al., 2005). The DN-cadherin EC9–EC10 linker region, like the DE-cadherin EC2–EC3 linker region, was predicted to be devoid of Ca^{2+}-binding insertions (Jin et al., 2012; Fig. S1), raising the possibility of a bent or folded conformation. Our results with the DE-cadherin–DN-cadherin hybrid construct D1N9-11 (Fig. 3C; Fig. 5D–F) support the idea that that type IV and type III cadherins might share, at least in part, the structural mechanisms responsible for binding specificities. However, it is important to note that, as the D1N9-11 construct is not capable of mediating homophilic adhesion by itself, the DN-cadherin EC9–EC11 region is not guaranteed to recognize the same region of the intact DN-cadherin. Therefore, the possibility of heterophilic interactions between different extracellular cadherin domains of the same type III cadherins should be considered. As previously discussed, type III cadherin has been suggested to represent the ancestral 'E-cadherin' owing to its presence at epithelial adherens junctions in certain animals (Hiroki, 2012). Future studies should focus on the question of how the ancestral classical cadherin instead utilized a large number of extracellular cadherin domains for adhesion and adherens junction architecture.

Interactions of classical cadherin ectodomains in the extracellular space between opposing membranes form the architectural basis of adherens junctions (Harrison et al., 2011), which are the key contributors to animal morphogenesis (Guillot and Lecuit, 2013; Takeichi, 2014). The evolution of the structural strategies for classical cadherin homophilic binding might have had an impact on the physical and mechanical properties of adherens junctions themselves and potentially on morphogenetic mechanisms as well. Additional studies on such epithelial mechanisms will be required for a deeper understanding of the varied morphological outcomes of animal evolution.

MATERIALS AND METHODS

DNA construction

A DNA fragment encoding the N-terminal 733-amino-acid region of DE-cadherin (amino acids 1–733) was amplified by PCR using the *Eco*RI-site-tagged primer (5′-GGGAATTCATGTCCACCAGTGTCCAGCGAATG-3′) and the *Xba*I-site-tagged primer (5′-GCTCTAGACAGGAACGGAG-CATTGTC-3′). This DNA fragment was cloned into pAc5.1/V5-His A (Invitrogen) using the *Eco*RI and *Xba*I sites, and the resultant plasmid was designated pAc-DEEC6-His.

A DNA fragment encoding the N-terminal 733-amino-acid region of DE-cadherin (amino acids 1–733) was amplified by PCR using the *Bsp*HI-site-tagged primer (5′-CATGTCATGAGCACCAGTGTCCAGCGAATG-3′) and the *Nhe*I-site-tagged primer (5′-CCTAGCTAGCCAGGAACGGAG-CATTGTC-3′). The *armadillo* region of pUP-Arm-EGFP (Oda et al., 2002) was replaced with this DNA fragment using the *Nco*I and *Nhe*I sites. The DE-cadherin–EGFP region of the resultant plasmid was amplified by PCR using the *Eco*RI-site-tagged primer (5′-GGGAATTCATGTCCACCAGT-GTCCAGCGAATG-3′) and the *Xba*I-site-tagged primer (5′-GCTCTAG-ACTTGTACAGCTCGTCCAT-3′). This DNA fragment was cloned into pAc5.1/V5-His A (Invitrogen) using the *Eco*RI and *Xba*I sites, and the resultant plasmid was designated pAc-DEEC6-EGFP-His.

Journal of Cell Science (2016) 129, 3309-3319 doi:10.1242/jcs.189258

A DNA fragment encoding the N-terminal 522-amino-acid region of DE-cadherin (amino acids 1–522) was amplified by PCR using the *Eco*RI-site-tagged primer (5′-GGGAATTCATGTCCACCAGTGTCCAGCGAATG-3′) and the *Xba*I-site-tagged primer (5′-GCTCTAGAGAAGTGCGGCTT-GTGGTC-3′). This DNA fragment was cloned into pAc5.1/V5-His A (Invitrogen) using the *Eco*RI and *Xba*I sites, and the resultant plasmid was designated pAc-DEEC4-His.

The DEFL and DNFL (pUAS-DN-cad) expression constructs were as described previously (Iwai et al., 1997; Oda and Tsukita, 1999). The entire coding sequence for Gb1-cadherin was amplified from *G. bimaculatus* embryonic cDNA by PCR using the *Nco*I-site-tagged primer (5′-CATGCCATGGAAGCTGTAATATTGTTC-3′) and the *Nhe*I-site-tagged primer (5′-CCTAGCTAGCACACCATGACTCAGATGCTG-3′). The *armadillo* region of pUP-Arm-EGFP was replaced with this DNA fragment using the *Nco*I and *Nhe*I sites, and the resultant plasmid designated pUP-Gb1FL. The *Nco*I-*Sma*I fragment isolated from pUP-Gb1FL was blunted by using Klenow fragment and cloned into pBluescript SK (+) using the *Sma*I site. An appropriate plasmid in which the Gb1-cadherin–EGFP fusion is encoded from the *Kpn*I side was selected and designated pBS-Gb1FL. The *Eco*RI fragment isolated from pBS-Gb1FL was transferred to the expression vector pUAST (Brand and Perrimon, 1993), resulting in the Gb1FL expression construct.

For generation of the hybrid constructs for DE-cadherin and Gb1-cadherin, pBS-DEFL (Oda and Tsukita, 1999) and pBS-Gb1FL were used as PCR templates, in combination with the In-Fusion HD Cloning Kit (Clontech). For each hybrid construct, two pairs of PCR primers (t1F-t1R, t2F-t2R) were designed as listed in Table S1. The products of PCR amplification with t1F and t1R from pBS-DEFL and with t2F and t2R from pBS-Gb1FL were used for the In-Fusion cloning reactions according to the manufacturer's protocol. The resulting hybrid constructs were transferred to pUAST. The hybrid constructs for DE- and Fc1-cadherins and for DE- and DN-cadherins were generated in the same manner using the primers and templates described in Table S1.

The entire coding sequence for mKate2 was amplified by PCR from pmKate2-H2B (Evrogen) using the *Eco*RI-site-tagged primers (5′-GGA-ATTCATGAGCGAGCTGATTAAGGAG-3′, 5′-GGAATTCTCATCTG-TGCCCCAGTTTGC-3′). This DNA fragment was cloned into the *Eco*RI site of pUAST, resulting in pUAST-mKate2. The entire coding sequence for TagBFP was amplified by PCR from pTagBFP-N (Evrogen) using the *Eco*RI-site-tagged primers (5′-GGAATTCATGAGCGAGCTGATTAAG-GAG-3′, 5′-GGAATTCTTAATTAAGCTTGTGCCCCAG-3′). This DNA fragment was cloned into the *Eco*RI site of pUAST, resulting in pUAST-TagBFP. pWA-GAL4 is a gift of Yasushi Hiromi (National Institute of Genetics, Japan), from which GAL4 is expressed by the actin promoter. PrimeSTAR HS DNA Polymerase (Takara) was used for the PCRs. All constructs were confirmed by sequencing.

Expression of the expected products from equal amounts of the constructed plasmids was confirmed by transient transfection and western blot analyses (Fig. S3). The antibodies used for western blot analyses are as follows: mouse monoclonal antibody to GFP (1:500, 8362-1; Clontech); rat monoclonal antibodies DCAD1 and DCAD2 to DE-cadherin (1:100 for both; Oda et al., 1994); mouse monoclonal antibody to *Drosophila* α-spectrin, 3A9 (323 or M10-2, 1:200 for both), which was deposited in the Developmental Studies Hybridoma Bank by D. Branton and R. Dubreuil; and guinea pig antiserum to Gb1-cadherin (1:400; Oda et al., 2005). Based on the reactivity to polypeptide products from random-primed DE-cadherin cDNA fragments (Oda et al., 1994) and to the DE-cadherin constructs described in this and previous work (Oda and Tsukita, 1999; Fig. S3), the epitopes of DCAD1 and DCAD2 were located within the amino acids 492–574 and 213–301 regions, respectively, of DE-cadherin.

Protein purification

To produce S2 cells stably expressing DEEC6–His, DEEC6–GFP–His, DEEC4–His or DEEC4–GFP–His, the expression plasmids were individually co-transfected with the pCoBlast selection vector into S2 cells, and stable cell lines were selected with blasticidin according to the manufacturer's protocol for the *Drosophila* expression system (Invitrogen). S2 cells stably expressing tagged DE-cadherin extracellular cadherin domains were seeded at a density of 1×10^6/ml in 10 ml Schneider's medium (Thermo Fisher Scientific) supplemented with 10% heat-inactivated fetal bovine serum, followed by 3–7 days of incubation. An 8-ml sample of the culture medium containing secreted His-tagged proteins was centrifuged at 400 ***g*** for 5 min at 4°C, and 5 ml supernatant was collected. The His-tagged Protein Purification Kit (Medical & Biological Laboratories) was used to purify the His-tagged proteins from the supernatants according to the manufacturer's instruction. The proteins were eluted with excess 6×His peptides (WAKO) in 40 µl HC buffer (20 mM HEPES, 4 mM $CaCl_2$, adjusted with NaOH to pH 7.35), which was stored at 4°C until use. Purified proteins were separated on 4–12% Bis-Tris Gels (Thermo Fisher Scientific) and analyzed by Coomassie Brilliant Blue staining and western blotting. Detection of purified proteins was performed using the rat monoclonal antibody DCAD2 (1:1000; Oda et al., 1994), ECL horseradish peroxidase (HRP)-conjugated anti-rat-IgG antibody (GE Healthcare) and ECL Prime Western Blotting Detection Reagent (GE Healthcare).

Preparation of purified proteins for AFM

A mica substrate with diameter of 1.5 mm and a thickness of 0.1 mm was attached with glue in the center of 15-mm-diameter hydrophilic circles on a glass slide. A total of 2 µl purified proteins in solution was adsorbed to freshly cleaved mica for 15 min at a density of ∼500 molecules/µm^2, and the mica surface was washed with one or two times with 400 µl HC buffer. These processes were conducted at room temperature (25°C). The concentration of the proteins used for adsorption was adjusted based on pilot observations.

AFM imaging

AFM imaging was performed in solution (HC buffer) using a tip-scan type AFM, BIXAM (Olympus), which was newly developed based on a previously described AFM imaging system (Suzuki et al., 2013). The AFM was set to phase modulation mode. We used the cantilevers BL-AC10FS (Olympus) with a length of 9 µm, a width of 2 µm and a thickness of 0.13 µm, or USC-F0.8-k0.1 (NanoWorld AG), a customized cantilever with a length of 9 µm, a width of 2 µm and a thickness of 0.10 µm. These cantilevers had a scanning tip radius of less than 10 nm, a resonant frequency in solution of 400 kHz, and a spring constant of 0.1 N/m. AFM imaging was performed at room temperature (25°C). We used a scanning area of 40×30 nm^2 with 192×144 pixels and a scanning speed of 1.8 µm/s for a high-resolution image (Fig. 1D), or a scanning area of 200×150 nm^2 or 400×300 nm^2 with 320×240 pixels and a scanning speed of 7.5–78 µm/s for other images (Fig. 1B,C,F,H-J; Fig. S2). AFM images were acquired at scanning rates of 0.05–0.2 fps and exported to bmp files. AFM images were processed and measured by ImageJ 1.49 g software (National Institutes of Health). Length measurements are represented as the means. A total of seven independent rounds of protein purification and AFM observation was performed for each of DEEC6–His and DEEC6–GFP–His and a total of two independent rounds for each of DEEC4–His and DEEC4–GFP–His. The tadpole-like configuration of DEEC6–His and DEEC6–GFP–His and the linear and variously bent configurations of DEEC4–His and DEEC4–GFP–His were confirmed in multiple experiments.

Cell aggregation assays

Drosophila S2 cells were cultured at 25°C in Schneider's insect medium (Sigma-Aldrich) supplemented with 10% heat-inactivated fetal bovine serum. For preparation of each cell population used in the cell aggregation assays, S2 cells were transiently transfected with a 5:5:1 mixture of pUAST-cadherin-X (where cadherin-X represents the construct of interest), pUAST-mKate2 or -TagBFP, and pWA-GAL4. Two days before cell aggregation assays, 5×10^6 S2 cells were plated per 100-mm dish and incubated for 6–8 h before transfection. Transfection was performed by the calcium phosphate co-precipitation method using a total of 11 µg plasmid DNA per dish. Half of the medium in each dish was replaced with fresh medium the next day. Approximately 42–45 h after transfection, the cells in each dish were harvested in a 15-mm tube, centrifuged (400 ***g*** for 5 min) and resuspended in 5 ml fresh medium supplemented with an addition of 4 µl 2.5 M $CaCl_2$ (raising the final concentration of Ca^{2+} to 7.4 mM from the original

Schneider's insect medium, which contained 5.4 mM $CaCl_2$). Repeated pipetting was used to separate the culture into single cells, which were used for cell aggregation assays.

To examine the homophilic binding activity of cadherin-X, 500 µl of a cell suspension containing cells expressing cadherin-X and mKate2 was added to a well in a 24-well microplate (1820-024; Iwaki). To examine the binding preferences of cadherin-X to DEFL, Gb1FL and DNFL, 100 µl of a cell suspension that contained cells simultaneously expressing cadherin-X and mKate2 and 400 µl of a cell suspension that contained cells simultaneously expressing DEFL, Gb1FL or DNFL, and TagBFP were added to a well in the 24-well microplate. To allow cell aggregation, the microplate was placed on a rotary platform at 150 rpm for 15 min at room temperature (25°C). Cell aggregates that formed in the wells were observed and photographed using an Olympus IX71 fluorescence microscope equipped with a UPlanFl 10×/N.A. 0.3 objective, differential interference contrast optics and a CoolSNAP HQ camera (Roper Scientific) that were controlled by Metamorph version 6.2 software (Molecular Devices). Chroma 8600 series multi-band filter sets [Exciter (Ex)555/28, Emitter (Em)617/73, Ex403/12, Em457/50, Ex490/20, and Em528/38] were used for sequential acquisition of 16-bit images for the fluorescence of mKate2, TagBFP and GFP. All data were acquired at the same parameter settings. Fluorescence images were analyzed using ImageJ 1.47 m software, and quantitative data were analyzed using OriginPro 2015 (OriginLab). To quantify the binding preference of each cadherin construct to DEFL, Gb1FL or DNFL, 128 µm×128 µm square regions (200 pixels×200 pixels) that captured cell aggregates identified by TagBFP fluorescence were randomly selected. The mean intensities of TagBFP and mKate2 fluorescence for the selected regions, were calculated after background subtraction. The ratio of the mKate2 to TagBFP fluorescence intensity was defined as the binding preference. Three independent experiments were performed for each cadherin construct. Preference values were normalized and represented as the means±s.e.m. The significance of the difference between the preference values of two related constructs was assessed using Welch's *t*-test. To prepare the images shown at the bottom of Fig. 3D, mKate2 fluorescence images were processed using the 'Find Edges' and 'Make Binary' functions at the default setting in ImageJ.

Cell aggregation assays as shown in Fig. 5A–C were performed in the same manner except for the following points: for preparation of a third cell population, S2 cells were transiently transfected with a 5:2.5:2.5:1 mixture of pUAST-cadherin-X, pUAST-mKate2, pUAST-TagBFP, and pWA-GAL4. For co-aggregation of the cell populations, 167 µl of each cell suspension was added to a well in the 24-well microplate.

Acknowledgements
We thank Y. Hiromi for the pWA-GAL4 plasmid; Y. Iwai and T. Uemura for the DN-cadherin expression plasmid; Y. Tsukasaki, Y. Uekusa, T. Haruta, M. Kanayama and Y. Akiyama-Oda for technical advice and discussion; A. Noda for technical assistance; other members of JT Biohistory Research Hall for discussion; the Developmental Studies Hybridoma Bank for antibodies; Y. Akiyama-Oda and S. Iwasaki for comments on the manuscript; S. Ito, T. Sato, and S. Karaki for supervision; and K. Nakamura for encouragement.

Competing interests
The authors declare no competing or financial interests.

Author contributions
S.N. and H.O. designed the experiments and performed the molecular and cellular experiments and data analysis. S.N., A.Y. and N.S. conducted the AFM imaging. S.N. and H.O. wrote the manuscript.

Funding
This research received no specific grant from any funding agency in the public, commercial, or not-for-profit sectors.

Supplementary information
Supplementary information available online at
http://jcs.biologists.org/lookup/doi/10.1242/jcs.189258.supplemental

References
Becker, J. W., Erickson, H. P., Hoffman, S., Cunningham, B. A. and Edelman, G. M. (1989). Topology of cell adhesion molecules. *Proc. Natl. Acad. Sci. USA* **86**, 1088-1092.

Boggon, T. J., Murray, J., Chappuis-Flament, S., Wong, E., Gumbiner, B. M. and Shapiro, L. (2002). C-cadherin ectodomain structure and implications for cell adhesion mechanisms. *Science* **296**, 1308-1313.

Borghi, N., Sorokina, M., Shcherbakova, O. G., Weis, W. I., Pruitt, B. L., Nelson, W. J. and Dunn, A. R. (2012). E-cadherin is under constitutive actomyosin-generated tension that is increased at cell-cell contacts upon externally applied stretch. *Proc. Natl. Acad. Sci. USA* **109**, 12568-12573.

Brand, A. H. and Perrimon, N. (1993). Targeted gene expression as a means of altering cell fates and generating dominant phenotypes. *Development* **118**, 401-415.

Brasch, J., Harrison, O. J., Ahlsen, G., Carnally, S. M., Henderson, R. M., Honig, B. and Shapiro, L. (2011). Structure and binding mechanism of vascular endothelial cadherin: a divergent classical cadherin. *J. Mol. Biol.* **408**, 57-73.

Guillot, C. and Lecuit, T. (2013). Mechanics of epithelial tissue homeostasis and morphogenesis. *Science* **340**, 1185-1189.

Harris, T. J. C. and Tepass, U. (2010). Adherens junctions: from molecules to morphogenesis. *Nat. Rev. Mol. Cell Biol.* **11**, 502-514.

Harrison, O. J., Bahna, F., Katsamba, P. S., Jin, X., Brasch, J., Vendome, J., Ahlsen, G., Carroll, K. J., Price, S. R., Honig, B. et al. (2010). Two-step adhesive binding by classical cadherins. *Nat. Struct. Mol. Biol.* **17**, 348-357.

Harrison, O. J., Jin, X., Hong, S., Bahna, F., Ahlsen, G., Brasch, J., Wu, Y., Vendome, J., Felsovalyi, K., Hampton, C. M. et al. (2011). The extracellular architecture of adherens junctions revealed by crystal structures of type I cadherins. *Structure* **19**, 244-256.

Haruta, T., Warrior, R., Yonemura, S. and Oda, H. (2010). The proximal half of the *Drosophila* E-cadherin extracellular region is dispensable for many cadherin-dependent events but required for ventral furrow formation. *Genes Cells* **15**, 193-208.

Häussinger, D., Ahrens, T., Aberle, T., Engel, J., Stetefeld, J. and Grzesiek, S. (2004). Proteolytic E-cadherin activation followed by solution NMR and X-ray crystallography. *EMBO J.* **23**, 1699-1708.

Heisenberg, C.-P. and Bellaïche, Y. (2013). Forces in tissue morphogenesis and patterning. *Cell* **153**, 948-962.

Hiroki, O. (2012). Evolution of the cadherin–catenin complex. *Subcell. Biochem.* **60**, 9-35.

Hulpiau, P. and van Roy, F. (2009). Molecular evolution of the cadherin superfamily. *Int. J. Biochem. Cell Biol.* **41**, 349-369.

Hulpiau, P. and van Roy, F. (2010). New insights into the evolution of metazoan cadherins. *Mol. Biol. Evol.* **28**, 647-657.

Iwai, Y., Usui, T., Hirano, S., Steward, R., Takeichi, M. and Uemura, T. (1997). Axon patterning requires DN-cadherin, a novel neuronal adhesion receptor, in the Drosophila embryonic CNS. *Neuron* **19**, 77-89.

Jin, X., Walker, M. A., Felsövályi, K., Vendome, J., Bahna, F., Mannepalli, S., Cosmanescu, F., Ahlsen, G., Honig, B. and Shapiro, L. (2012). Crystal structures of *Drosophila* N-cadherin ectodomain regions reveal a widely used class of Ca^2+-free interdomain linkers. *Proc. Natl. Acad. Sci. USA* **109**, E127-E134.

Miller, J. R. and McClay, D. R. (1997). Characterization of the role of cadherin in regulating cell adhesion during sea urchin development. *Dev. Biol.* **192**, 323-339.

Miller, P. W., Clarke, D. N., Weis, W. I., Lowe, C. J. and Nelson, W. J. (2013). The evolutionary origin of epithelial cell–cell adhesion mechanisms. *Curr. Top. Membr.* **72**, 267-311.

Nagar, B., Overduin, M., Ikura, M. and Rini, J. M. (1996). Structural basis of calcium-induced E-cadherin rigidification and dimerization. *Nature* **380**, 360-364.

Nose, A., Tsuji, K. and Takeichi, M. (1990). Localization of specificity determining sites in cadherin cell adhesion molecules. *Cell* **61**, 147-155.

Oda, H. and Takeichi, M. (2011). Evolution: structural and functional diversity of cadherin at the adherens junction. *J. Cell Biol.* **193**, 1137-1146.

Oda, H. and Tsukita, S. (1999). Nonchordate classic cadherins have a structurally and functionally unique domain that is absent from chordate classic cadherins. *Dev. Biol.* **216**, 406-422.

Oda, H., Uemura, T., Harada, Y., Iwai, Y. and Takeichi, M. (1994). A *Drosophila* homolog of cadherin associated with armadillo and essential for embryonic cell-cell adhesion. *Dev. Biol.* **165**, 716-726.

Oda, H., Wada, H., Tagawa, K., Akiyama-Oda, Y., Satoh, N., Humphreys, T., Zhang, S. and Tsukita, S. (2002). A novel amphioxus cadherin that localizes to epithelial adherens junctions has an unusual domain organization with implications for chordate phylogeny. *Evol. Dev.* **4**, 426-434.

Oda, H., Tagawa, K. and Akiyama-Oda, Y. (2005). Diversification of epithelial adherens junctions with independent reductive changes in cadherin form: identification of potential molecular synapomorphies among bilaterians. *Evol. Dev.* **7**, 376-389.

Overduin, M., Harvey, T. S., Bagby, S., Tong, K. I., Yau, P., Takeichi, M. and Ikura, M. (1995). Solution structure of the epithelial cadherin domain responsible for selective cell adhesion. *Science* **267**, 386-389.

Patel, S. D., Ciatto, C., Chen, C. P., Bahna, F., Rajebhosale, M., Arkus, N., Schieren, I., Jessell, T. M., Honig, B., Price, S. R. et al. (2006). Type II cadherin

ectodomain structures: implications for classical cadherin specificity. *Cell* **124**, 1255-1268.

Pokutta, S., Herrenknecht, K., Kemler, R. and Engel, J. (1994). Conformational changes of the recombinant extracellular domain of E-cadherin upon calcium binding. *Eur. J. Biochem.* **223**, 1019-1026.

Shapiro, L., Fannon, A. M., Kwong, P. D., Thompson, A., Lehmann, M. S., Grübel, G., Legrand, J. F., Als-Nielsen, J., Colman, D. R. and Hendrickson, W. A. (1995). Structural basis of cell-cell adhesion by cadherins. *Nature* **374**, 327-337.

Suzuki, Y., Sakai, N., Yoshida, A., Uekusa, Y., Yagi, A., Imaoka, Y., Ito, S., Karaki, K. and Takeyasu, K. (2013). High-speed atomic force microscopy combined with inverted optical microscopy for studying cellular events. *Sci. Rep.* **3**, 2131.

Takeichi, M. (1990). Cadherins: a molecular family important in selective cell-cell adhesion. *Annu. Rev. Biochem.* **59**, 237-252.

Takeichi, M. (1991). Cadherin cell adhesion receptors as a morphogenetic regulator. *Science* **251**, 1451-1455.

Takeichi, M. (2014). Dynamic contacts: rearranging adherens junctions to drive epithelial remodelling. *Nat. Rev. Mol. Cell Biol.* **15**, 397-410.

Tanabe, K., Takeichi, M. and Nakagawa, S. (2004). Identification of a nonchordate-type classic cadherin in vertebrates: chicken Hz-cadherin is expressed in horizontal cells of the neural retina and contains a nonchordate-specific domain complex. *Dev. Dyn.* **229**, 899-906.

Tsukasaki, Y., Miyazaki, N., Matsumoto, A., Nagae, S., Yonemura, S., Tanoue, T., Iwasaki, K. and Takeichi, M. (2014). Giant cadherins Fat and Dachsous self-bend to organize properly spaced intercellular junctions. *Proc. Natl. Acad. Sci. USA* **111**, 16011-16016.

Vendome, J., Felsovalyi, K., Song, H., Yang, Z., Jin, X., Brasch, J., Harrison, O. J., Ahlsen, G., Bahna, F., Kaczynska, A. et al. (2014). Structural and energetic determinants of adhesive binding specificity in type I cadherins. *Proc. Natl. Acad. Sci. USA* **111**, E4175-E4184.

Vesenka, J., Manne, S., Giberson, R., Marsh, T. and Henderson, E. (1993). Colloidal gold particles as an incompressible atomic force microscope imaging standard for assessing the compressibility of biomolecules. *Biophys. J.* **65**, 992-997.

Yang, F., Moss, L. G. and Phillips, G. N. (1996). The molecular structure of green fluorescent protein. *Nat. Biotechnol.* **14**, 1246-1251.